

A novel process and thermodynamic mechanisms of air gap formation for ULSI application

Kow-Ming Chang*, Ji-Yi Yang, Lih-Woen Chen, Ming Hau Tseng

Department of Electronics Engineering & Institute of Electronics, National Chiao-Tung University, 1001 Ta-Hsueh Road, Hsinchu, Taiwan, PR China

Received 4 September 1999; received in revised form 14 June 2000; accepted 20 June 2000

Abstract

In this study, a novel process to fill the gap between the metal lines on a wafer with air is developed. Reduction of the parasitic wire capacitance in ULSI has become an important issue for future high-speed and low-power applications. Use of low dielectric constant material as inter-level dielectric (ILD) can overcome this problem. Many new low dielectric constant materials are under study and lower dielectric constant and feasibility are the two goals of these researches. The gas-dielectric process has the lowest dielectric constant, 1.0, and its conceptual feasibility is demonstrated. Basic process characterization data, thermodynamic mechanism and requirements for air gap formation are also discussed. We calculated the relationship among the surface tension, the vaporization rate and atmospheric pressure to construct a model of the process window to show that this process is feasible and reproducible. Scanning electron microscope data show that a large area of air gap can be obtained. Basic electrical characteristics data such as I–V and C–V, measured and compared with the conventional PECVD process, show that the air gap has better isolation than PECVD process. © 2000 Elsevier Science S.A. All rights reserved.

Keywords: Low dielectric constant material; ULSI; Gas-dielectric process; Low power

1. Introduction

As the feature sizes of ULSI technology continue to shrink, it is necessary to decrease the spaces between the neighboring metal lines and to adopt a multilevel interconnect to accommodate the increasing functional complexity of the electronic circuit. Consequently, the interconnect RC time constant delay will increase rapidly and become a major limiting factor in circuit performance. In recent years, many studies [1–3] have been performed on the low dielectric constant materials, which are used to fill the spaces between the metal

lines. Using low dielectric constant materials for the ILD, the space between the metal lines can be decreased without increasing parasitic capacitance. Low dielectric materials include fluorinated inorganic materials, porous silica, porous organic materials, and various organic materials, which can be deposited using spin-on or chemical vapor deposition techniques. In these low dielectric constant materials, only a few materials, such as FO_x , are approved for current production use; the other materials are still undergoing research.

Air has the lowest dielectric constant. A related technology, Air Bridge, using air as the ILD, is extensively applied in compound devices. However, the feasibility of fabrication and correspondent electrical reliability is still a huge problem in applying this technology to IC manufacturing. Some authors announced

* Corresponding author. Tel.: +886-3-5712121, ext. 31887; fax: +886-3-5731887.
E-mail address: kmchang@cc.nctu.edu.tw (K. Chang).

that they could form the air gap [4,5] in 1996–1997. Although, they professed that there were some problems that needed to be solved, the air gap with characteristics, such as low leakage current, low parasitic capacitance, made great progress in the ULSI interconnection field. The authors also discussed the thermal conduction problems of the air gap in a recent publication [6]. It was shown that the conductor lines played a most important role in thermal conduction. These studies indicated that the air gap is feasible in manufacturing. In this paper, a novel process to form the air gap and the electrical characteristics of air gap are proposed. Compared to the previous technologies, this technology can form an air gap with a simpler process and lower cost. Furthermore, its bridge layer is formed with a low-dielectric material, which enables the advantage of low parasitic capacitance.

2. Experimental

2.1. Traditional process flow

There are two kinds of traditional technologies used to fill a space with inter-level dielectric material. One process uses spin-on technology to coat ILD on a patterned wafer. After the spin-on deposition, the wafer is baked, and cured. The low dielectric constant materials fill in the gaps between metal lines. At the same time, the planarization of the wafer is completed. Sometimes, a two-step spin-on process is needed to produce global planarization [7]. The other process used to fill the ILD spaces is to deposit PECVD oxide onto the patterned metal lines followed by the chemical–mechanical polishing (CMP) process to produce a planar surface.

2.2. New process flow

The proposed process flow is described schematically in Fig. 1. There are four steps to form the air gap. First, a silicon nitride film is deposited on silicon wafer, patterned with special layout, coated with polyimide and baked at 90°C for 3 min. The special layout patterns silicon nitride film to some silicon nitride beetle regions whose thickness, h , is thicker than the interconnect lines (1.08 μm). In this step, the silicon beetle regions should be located far away from the metal lines region to avoid affecting the flowage of $\text{FO}_x\text{-16}$, for example, the four corners of the patterned interconnect metal line. The polyimide type is Dupont PI 2809, which has better adhesion to a Si wafer than oxide when it is dry. Second, another wafer with a patterned metal layer TiN/Al-Si-Cu/TiN/Ti (40 nm/900 nm/100 nm/40 nm) sitting on a 500-nm SiO_2 layer on a Si substrate is prepared. The pattern is a cross-finger

structure. There are five hundred metal lines on each side. The widths of the lines are 0.5 μm and the sizes of the spaces between the lines are 0.5 μm , 0.7 μm and 1 μm , respectively. The residual photo-resist is removed using oxygen plasma ashing and MS-2001. The wafer prepared in step 2 is then slit into pieces of 9 cm^2 and faced downward on the top of the wafer prepared in step 1, and the two wafers are tilted an angle θ , e.g. approximately 45° used here. The 45° tilt is not critical for the processing. Next, $\text{FO}_x\text{-16}$ [7,8], inorganic hydrogen silsesquioxane [9], produced by the Dow Corning Corporation for ILD applications, is trickled through a slit between the patterned metal lines and the polyimide. The slit is produced in this step as shown in Fig. 1c. The height of the slit is equal to the thickness of silicon nitride beetle region minus the thickness of the metal line. This process is operated in atmospheric pressure. No special gas environment is used. Here, on silicon wafer prepared in step 1, the polyimide is diluted and the thickness of polyimide film above silicon nitride is supposed to be equal to the thickness of polyimide film above silicon substrate. Inside the slit, the liquid $\text{FO}_x\text{-16}$ flows along the planar polyimide surface and forms a planar surface in contact with the polyimide film. The thin liquid $\text{FO}_x\text{-16}$ is also in contact with the top of the metal lines and adheres to the metal lines. Here, the adhesion force between the top of the metal lines and the $\text{FO}_x\text{-16}$ is stronger than the adhesion force between the $\text{FO}_x\text{-16}$ and the polyimide. The same process is repeated with different ratios of methyl isobutyl ketone (MIBK) to $\text{FO}_x\text{-16}$. The ratios of $\text{FO}_x\text{-16}$ to MIBK used were 1:1, 1:3, 1:5 and 1:10, respectively. The MIBK is the carrier solvent of $\text{FO}_x\text{-16}$, flowable oxide, which can escape in vapor at room temperature. Finally, we can scratch the polyimide film from the oxide or dissolve the polyimide film to separate the two wafers and obtain the air gap.

3. Results and discussion

There are three components in this discussion. The first component involves the basic characteristics of this material, $\text{FO}_x\text{-16}$. Recording and analyzing the data will help us to understand the creation of the air gap. The second component involves mathematic calculations used to construct the model for processing the air gap window. This work will give us a quantitative model of this process. Based on this model, the other solvents meeting the conditions in this model will have the same effect as $\text{FO}_x\text{-16}$. The third component involves the basic electrical characteristics. PECVD oxide was chosen as the experimental control for the air gap. The experimental data show that the air gap structure has a lower leakage current and less parasitic capacitance.

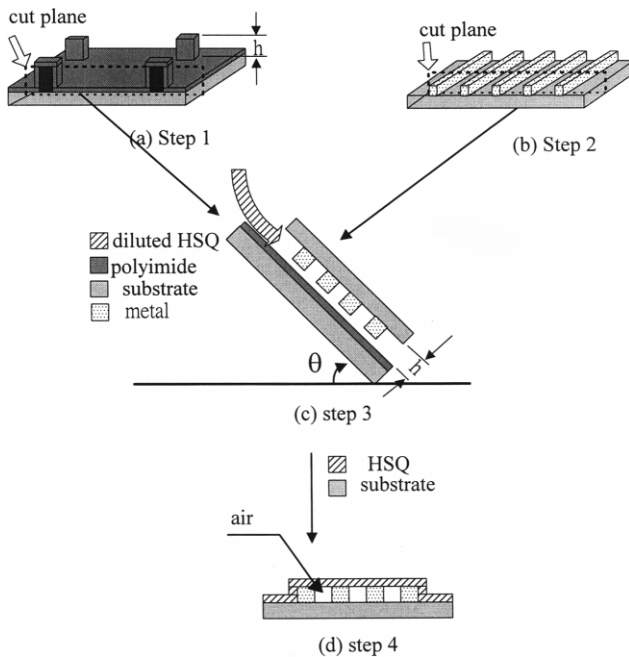


Fig. 1. New method to form air gap with flowable oxide.

3.1. The basic material characteristics of the flowable oxide (FO_x-16)

FO_x-16 is composed of 22% solid content and 78% solvent. This solvent evaporates easily at room temperature. After vaporization of the solvent, the FO_x-16 becomes a gel and cannot flow like a liquid. During the change from liquid into gel, FO_x-16 loses approximately 30% of its volume. The FO_x-16 gel still abounds with solvent. Baking is always used to remove the residual solvent. Fig. 2 shows the thickness variations in the polyimide in various ratio of FO_x-16 to MIBK. There are two conditions plotted, before baking and after baking. In the case of before baking, the FO_x-16 with lower ratios of MIBK has higher thickness. For example, the thickness of dry FO_x-16 is approximately 2000 nm and the thickness of dry FO_x-16 with ratio 10:1 is approximately 200 nm. The same situation is observed in the case of after baking. We also measured the vaporization speed of MIBK and FO_x-16 . The process was experimented on the window of the wet bench. A rotator was used in the beaker to accelerate the evaporation. The weight of the sample was measured periodically to determine the evaporated amount of solvent. From the experimental data, we determined that the vaporization rate for FO_x-16 was higher than MIBK. The vaporization speeds for the MIBK and FO_x-16 were $0.475 \mu\text{m/s}$ and $0.657 \mu\text{m/s}$, respectively. Fig. 3 shows the surface tension. The data for MIBK and FO_x-16 were measured while the calculations for the other three materials are from the published data [10]. The common phenomenon associated with surface ten-

sion is the rise (or fall) of a liquid in a capillary tube. When the attraction (adhesion) between the wall of the tube and liquid molecules is strong enough to overcome the mutual attraction (cohesion) of the molecules, the surface tension pulls the molecules up the wall. The height, h , is determined by the relationship [11]

$$h = \frac{2\sigma\cos\theta}{\gamma R} \quad (1)$$

where σ is the surface tension, R is the tube radius, θ is the *angle of contact*, and is a function of both the liquid and the surface, γ is the specific weight of the liquid defined as the product of the acceleration of gravity, g , and density, ρ . It was observed that the pure solvent, MIBK, has a higher surface tension than FO_x-16 . Densities of MIBK and FO_x-16 are measured, too. The higher density will have a lower height as shown in Eq. (1). The density of FO_x-16 and MIBK is 0.886 g/ml, and 0.771 g/ml, respectively. Fig. 4 shows the SEM picture in which the FO_x-16 forms the bridge layer on the top of the metal lines. In Fig. 4, the upper regions were metal lines and thin insulator films, which formed the ‘bridge layer’ over interconnection metal lines. The dark squares and bright columns shown on the middle are ‘air’ and metal lines, respectively. The ‘air’ regions are formed by the mixture of the volatile matter of FO_x-16 and the surrounding air in process. Each sample is baked at 180°C for 3 min and cured at 400°C for 30 min. No cracks are observed. In Fig. 4, a lower concentration of FO_x-16 was used, so the bridge layer is thinner. In our samples, the thickness of the bridge layer can be changed from 50 nm to 300 nm by using different concentrations of FO_x-16 and different slit heights. In only a few conditions, the bridge layers are not so smooth as shown in Fig. 4. This effect can be overcome by depositing plasma enhanced chemical vapor deposition (PECVD) oxide over the bridge layer and CMP process. In our observation, the process is rather uniform all over the sample.

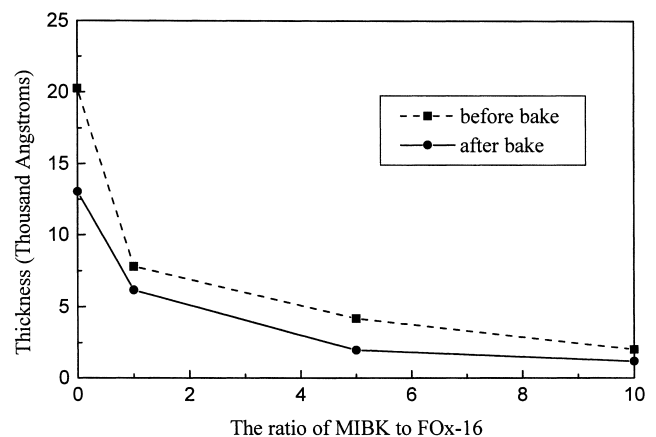


Fig. 2. The thickness variation vs. the ratio of MIBK to FO_x-16 .

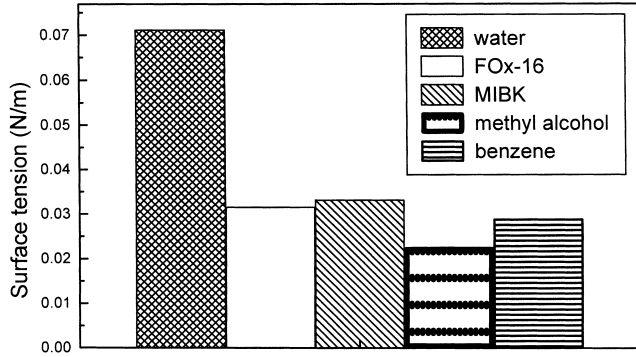


Fig. 3. Surface tension of MIBK, FO_x-16 and other solvents.

3.2. The thermodynamic model of the air gap formation

According to the data measured in part A and some concepts from fluid mechanics, we can divide step 4 of the process into two steps to explain the formation of the air gap.

Part 1: The diluted FO_x-16 is trickled through the slit and forms an ultra thin liquid layer between the polyimide surface and the top of the metal lines.

In this part, different ratios of MIBK to FO_x-16 will form a different thickness of liquid layers as shown in Fig. 2. Comparing the unbaked thickness with the baked thickness, we can also determine that a thicker FO_x-16 layer will require more solvent to be removed in the baking step.

Part 2: In this part, we assumed that the space between the metal lines and the liquid layer can be open or closed and calculate their respective effects. In the assumption of a closed space, atmospheric pressure is considered.

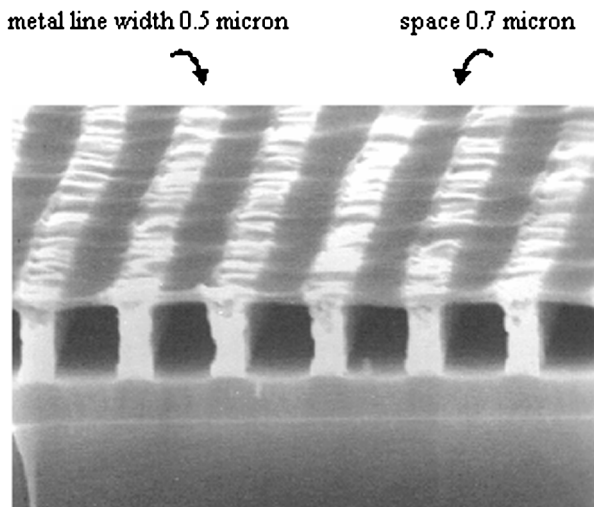


Fig. 4. Air gap with bridge layer of FO_x-16.

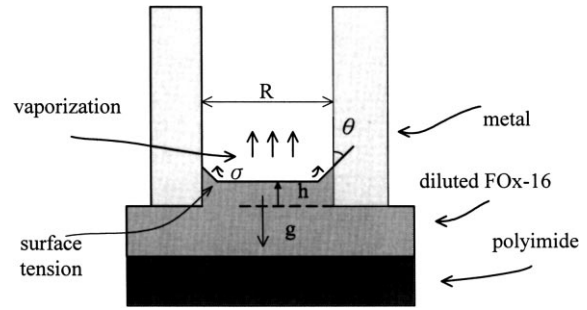


Fig. 5. Surface tension of diluted FO_x-16 pulls the surface up and the solvent evaporates at the surface simultaneously.

3.2.1. Open space

First we consider that the space between the metal lines is open. The surface tension between the wall of the metal lines and the liquid layer pulls the surface of the liquid layer up and the solvent inside the liquid layer evaporates at the same time. On the other side, the weight of the liquid pulls the surface of the liquid layer down as shown in Fig. 5. In the test structure, these respective effects can be shown [11]:

$$F_{down} = Rlh\gamma \quad F_{up} = 2l\sigma\cos\theta \quad (2)$$

where R is the space between the metal lines, l is the length of the metal line, σ is the surface tension, θ is the angle of contact, h is the height of the liquid, a function of the time, and γ is the product of density ρ and the acceleration of gravity g .

In a general case, the $\cos\theta$ is positive, the ascendant acceleration of the liquid surface then can be written as

$$a = \frac{2l\sigma\cos\theta - Rlh\gamma}{Rlh\rho}$$

or

$$a = \frac{2\sigma\cos\theta - Rh\gamma}{Rh\rho}$$

then

$$\Rightarrow \int_0^t \left(\frac{2\sigma\cos\theta}{Rh\rho} - g \right) t dt = h(t)$$

To simplify the equation, we define

$$k = \frac{2\cos\theta}{R\rho}$$

Then

$$\int_0^t \left(\frac{k\sigma}{h} - g \right) t dt = h(t)$$

Differentiate this equation on each side

$$\Rightarrow \left(\frac{k\sigma}{h} - g \right) t = h'(t)$$

then

$$\Rightarrow h dh = (k\sigma - gh) t dt$$

For simplicity, if we assume that k and σ are constant, then we can have

$$k\sigma - gh = u \Rightarrow h = (k\sigma - u) / g$$

$$dh = -du / g$$

this equation can be rewritten as

$$\frac{(k\sigma - u)(-du)}{ug^2} = t dt$$

$$\Rightarrow \frac{1}{g^2} \left(1 - \frac{k\sigma}{u} \right) du = t dt$$

Integrating the above equation

$$\Rightarrow \frac{1}{g^2} \left(\int du - \int \frac{k\sigma du}{u} = \int t dt \right)$$

Substituting the boundary condition $h = 0$ and $t = 0$ into Eq. (3)

$$\Rightarrow \frac{1}{g^2} (u - k\sigma \ln u) = \frac{1}{2} t^2 + c$$

$$\Rightarrow \frac{1}{g^2} [k\sigma - gh - k\sigma \ln(k\sigma - gh)] = \frac{1}{2} t^2 + C \quad (3)$$

We can obtain

$$C = 1/g^2 (k\sigma - k\sigma \ln k\sigma) \quad (4)$$

In a general condition, the solvent will not evaporate, so from Eq. (1)

$$h_{\max} = \frac{2\sigma \cos \theta}{\gamma R}$$

And the relationship between the height of the surface and time from Eqs. (3) and (4) can be rewritten as

$$\frac{1}{g^2} [k\sigma \ln(k\sigma) - gh - k\sigma \ln(k\sigma - gh)] = \frac{1}{2} t^2 \quad (5)$$

If we want to make the air gap, h_{\max} must be smaller than the height of the metal lines, e.g. 1.08 μm here.

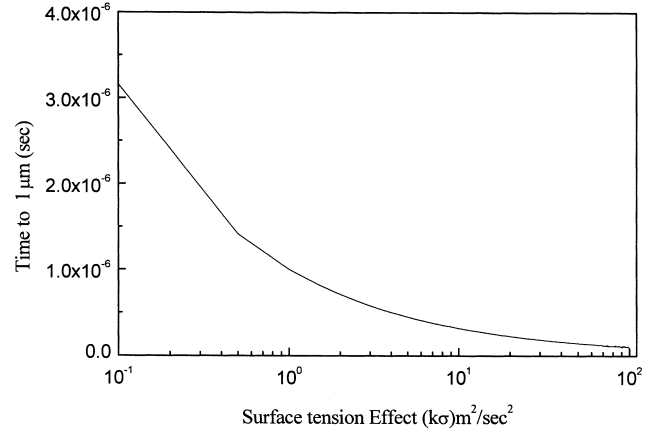


Fig. 6. The Curve of surface tension effect ($k\sigma$) vs. time for the liquid surface risen to 1 μm .

However, it is impossible for most solvents, for example, water at 20°C, the surface tension σ is 7.28×10^{-2} N/m, $\theta = 0$, R is 1 μm , and γ is 9.789 kN/m³, then the h_{\max} is 14.873 m.

Second, the vaporization of the solvent is considered. If we want to make an air gap, it is necessary that the liquid layer becomes to a gel before h approaches 1.08 μm . So

$$t[h = 1 \mu\text{m in (5)}] \geq t(\text{liquid becomes gel}) \quad (6)$$

To calculate the right side of Eq. (6), we use the data of vaporization speed and make some assumptions. For example, the vaporization rate is 0.65761 $\mu\text{m/s}$, and we assume that the liquid layer of the FO_x-16 is 1 μm and the gel of FO_x-16 is 0.7 μm . The right side of Eq. (6) is 0.4562 s. In a general case, the surface tension of the inorganic solvent is approximately one half to one third of water [10]. If θ is zero, R is 1 μm , $k\sigma$ is approximately 10–100, $k\sigma - gh$ is equal to $k\sigma$, and if Eq. (6) is correct, $k\sigma - gh$ must be smaller than 10–230 000. Eq. (5) is plotted in Fig. 6, the x -axis is $k\sigma$ and the y -axis is time. The black line in this figure represents the time that the liquid layer approaches 1 μm . Thus, θ must be greater than 90° to create the air gap. Otherwise, the FO_x-16 will flow into the gap.

3.2.2. Closed space

In a closed space, the liquid surface suffers forces as shown in Fig. 7. Because surface tension and the force of atmospheric pressure have larger effects than the vaporization of solvent to form air gap, in a closed space, we ignored the effect of vaporization. The force of atmospheric pressure and the liquid weight pull the liquid surface down, while the surface tension pulls the liquid surface up. If

$$F_{\text{atmospheric pressure}} + F_{\text{weight}} \geq F_{\text{surface tension}} \quad (7)$$

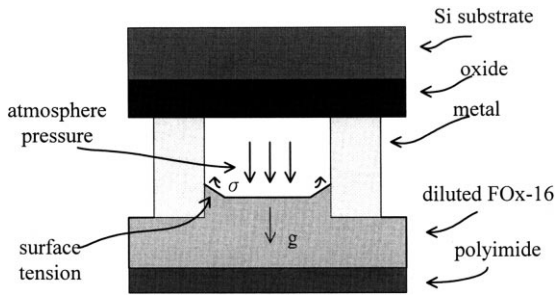


Fig. 7. In closed space, the height of liquid surface depends on surface tension and atmosphere pressure.

the liquid surface will not rise. In Eq. (7), if we substitute $F_{\text{atmospheric pressure}}$ with $1.01325 \times 10^5 \text{ N/m}^2$, and ignore the effect of the F_{weight} , we can obtain Fig. 8. The x -axis is the spacing of the metal lines, the y -axis is the force acting upon the liquid surface. The flat line is the atmospheric pressure, and the bent lines are the products of the surface tension and contact angle, which is supposed as zero, as shown in Eq. (2). If the flat line is higher than the bent line, the liquid surface will not rise and the height of the air gap is equal to the height of the metal lines.

3.3. The measurement of the electric characteristics

Fig. 9 shows the current leakage of our test structure. This indicates that the air gap has a better isolation effect than the PECVD oxide. These data are similar to those published by Anand et al. [4]. No breakdown phenomenon was observed before 30 V. Table 1 shows the parasitic capacitance of the air gap. The test structure is $0.7 \mu\text{m}/0.5 \mu\text{m}$ spacing/width with $1.08 \mu\text{m}$ height. The $\text{FO}_x\text{-16}$ -immersion height as shown in Fig. 5 is lower than 50 nm. The parasitic capacitance of a reference sample using $1 \mu\text{m}$ PECVD oxide as inter-layer dielectric constant is 34 fF/mm, which is approximately four times higher than that of

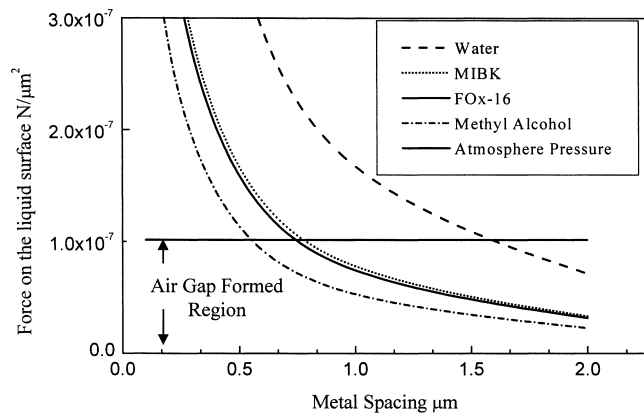


Fig. 8. Atmosphere pressure and force of surface tension on various liquids surface vs. metal spacing.

Table 1
Comparison of the parasitic capacitance of the air gap and plasma-TEOS ILD

Measured capacitance	
Plasma-TEOS ILD	Air gap
$C = 34 \text{ fF/mm}$	$C = 8.4 \text{ fF/mm}$

the air gap, 8.4 fF/mm. The measured parasitic capacitance is the average value of many measurements. This also indicates that the air gap has a lower capacitance, which allows more potential for high-speed circuits.

4. Conclusion

We developed a novel process to form air gap. Its key technology involves the use of the flowable property of a low dielectric material to form an ultra-thin liquid layer while contacting with the top of the metal lines. Using solvents with appropriate surface tension, we can utilize atmospheric pressure to prevent the liquid low dielectric material from flowing into the gaps between the metal lines. Scanning electron microscope pictures show that this technology can form a planar surface and air gap. With the experimental data and mathematical calculations, we constructed a thermodynamic model to describe the process window of the air gap. This process is simple and inexpensive. The air gap has lower current leakage and parasitic capacitance. We believe that for higher speed circuits, this technology will gain more and more importance.

Acknowledgements

This work is supported by National Nano Device Laboratory in Hsin-Chu, Taiwan under NSC-87-2215-E009-071. Thanks also to Dow Corning Cooperation for their $\text{FO}_x\text{-16}$ material support.

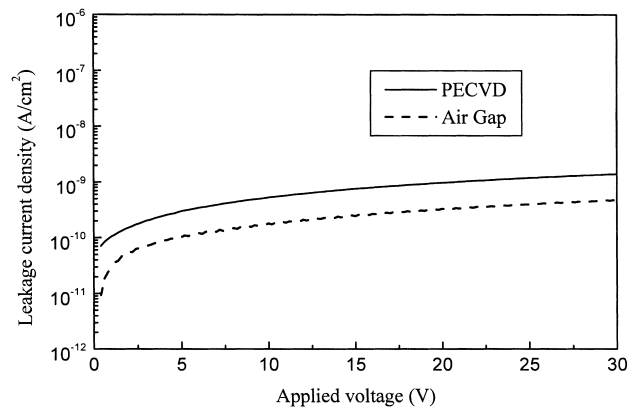


Fig. 9. Wire-to-wire isolation characteristics with $0.7/0.5 \mu\text{m}$ spacing/width.

References

- [1] B. Roberts, A. Harrus, R.L. Jackson, *Solid State Technol.* 38 (1995) 69.
- [2] Zhao, S.Q. Wang, S. Anderson, R. Lam, M. Fiebig, P.K. Vasudev, T.E. Seidel, in: K.N. Tu, J.M. Poate, L.J. Chen (Eds.), *Advanced Metallization for Future ULSI*, San Francisco, USA, 8–11 April 1996, Materials Research Society Symposium Proceeding 427 (1996) 83.
- [3] S.P. Murarka, *Solid State Technol.* 39 (1996) 83.
- [4] M.B. Anand, M. Yamada, H. Shibata, *IEDM Tech. Dig.* (1996) 82.
- [5] J.G. Fleming, E. Roferty-Osmun, in: *Proceedings of the Third International Dielectrics for ULSI Multilevel Interconnection Conference (DUMIC)*, Santa Clara, CA, 10–11 February 1997, p. 139.
- [6] M.B. Anand, M Yamada, H. Shibata, *IEEE Trans. Electron Devices* 44 (1997) 1965.
- [7] D. Thomas, G. Smith, L. Nauyen, in: *Proceedings of the Third International Dielectrics for ULSI Multilevel Interconnection Conference (DUMIC)*, Santa Clara, CA, 10–11 February 1997, p. 361.
- [8] J.N. Bremmer, Y. Liu, K.G. Gruszynski, F.C. Dall, in: *Proceedings of the Third International Dielectrics for ULSI Multilevel Interconnection Conference (DUMIC)*, Santa Clara, CA, 10–11 February 1997, p. 333.
- [9] J. Goo, B.K. Hwang, J.H. Choi, U-In Chung, Y.B. Koh, in: *Proceedings of the Third International Dielectrics for ULSI Multilevel Interconnection Conference (DUMIC)*, Santa Clara, CA, 10–11 February 1997, p. 329.
- [10] R.W. Fox, A.T. McDonald, *Introduction to Fluid Mechanics*, Wiley, New York, 1992.
- [11] B.R. Munson, D.F. Young, T.H. Okiishi, *Fundamentals of Fluid Mechanics*, John Wiley & Sons, Inc, 1990.